Journal of The Electrochemical Society, **147** (6) 2380-2384 (2000)
S0013-4651(99)08-061-1 CCC: $7.00

Characterization of Yttria-Stabilized Zirconia Thin Films Prepared by Radio Frequency Magnetron Sputtering for a Combustion Control Oxygen Sensor

J. W. Bae,[a,z] J. Y. Park,[a] S. W. Hwang,[a] G. Y. Yeom,[a,*] K. D. Kim,[b] Y. A. Cho,[b] J. S. Jeon,[b] and D. Choi[b,*]

[a]*Department of Materials Engineering, Sungkyunkwan University, Suwon 440-746, Korea*
[b]*Korea Gas Corporation 638, Research and Development Center, Ansan 425-150, Korea*

8 mol %-yttria-stabilized zirconia (YSZ) thin films as an oxygen ion conductor were deposited by radio frequency magnetron sputtering, and the oxygen gas sensing properties of YSZ were investigated using the structure of SiO_2 substrate/Ni-NiO/Pt/YSZ/Pt. X-ray diffractometry was employed to study the structure of YSZ and Ni-NiO films, and energy dispersion X-ray was used to investigate the composition of Ni-NiO thin films. The gas-sensing test was carried out for a SiO_2/Ni-NiO/Pt/YSZ/Pt film structure exposed to oxygen-controlled environments. The steady-state electromotive force (EMF) values were measured as a function of oxygen partial pressure (p_{O_2}; 1.013×10^3 to 1.013×10^5 Pa) and operating temperature (573 to 973 K). The fabricated gas sensor cells showed good oxygen sensing properties at the temperature range from 673 to 773 K. However, the sensors were unstable at the operational temperatures above 873 K possibly due to the enhanced interdiffusion of the materials in the multilayer. Also the operation of the sensor at temperatures below 573 K was not good because the temperature was not sufficient to cause ionic conduction in the cell. At the optimum temperature range, the experimental EMF values measured as a function of oxygen partial pressure were close to the theoretically calculated EMF values.

Manuscript submitted August 17, 1999; revised manuscript received February 10, 2000.

Yttria-stabilized zirconia, a well known oxygen ion conductor, is one of the many solid-state ionic materials utilized in the variety of electrochemical devices including fuel cells, oxygen pumps, and chemical gas sensors because of a number of superior properties such as heat resistance, high hardness, chemical durability, and high oxygen ionic conductivity.[1,2] It is also used as a buffer layer to deposit thin films of high-temperature superconductors on the substrates such as silicon, alumina, and sapphire. Bulk-type YSZ oxygen sensors especially have been widely used for combustion control in heat-treatment furnaces, glass tank furnaces, ceramic kilns, boilers, and gas stoves and also for oxygen control in steel and copper melts. However, the largest single use of general oxygen sensors is in automobiles for improving the fuel efficiency and for controling H_2, CO, and NO_x content in the exhaust gas.[3-6]

The carrier transport mechanism of YSZ is known to be the ionic conduction through oxygen vacancies. These vacancies are formed mainly as a result of the electroneutrality requirement with the presence of about 8-10 mol % of stabilizing dopants such as Y_2O_3, CaO, or MgO, that is, oxide compounds containing cations with a valence lower than Zr. [7,8] It appeared to be desirable to use materials with maximum disorder for solid electrolytes to achieve high conductivity for practical applications and the fabrication of YSZ thin-film-based oxygen sensor cells, and its oxygen sensing properties have not been reported yet.

Commercially available YSZ oxygen gas sensors rely on the traditional bulk ceramic fabrication. However, if the YSZ could be applied as a thin film, it would offer many advantages including compact dimensions with smaller power consumption, reduced ohmic losses, lower operating temperatures, etc., including the ease of mass fabrication using semiconductor fabrication techniques. Also, bulk sensors should show decreased gas sensing effects as compared with thin-film sensors at the same temperature because of the long path of the oxygen ion in the solid electrolyte. Therefore, to get the gas sensing properties with the bulk sensors, a high temperature operation of 873~1073 K is required for the oxygen ions to be appreciably mobile. However, thin-film sensors would show comparable gas sensing characteristics at lower temperatures than bulk sensors due to the decrease in ohmic resistance of the solid electrolyte with decreasing the thickness.[9-11]

YSZ thin films have been deposited for thin-film fuel cells by a number of techniques such as sol-gel, spray pyrolysis, evaporation, chemical vapor deposition (CVD), and radio frequency (rf) sputtering.[12-18] Among these techniques, the rf magnetron reactive sputtering technique offers better stoichiometry of the film in addition to the advantage of controlling oxygen atomic percent in YSZ thin films. Also, dc reactive sputtering has been used successfully for the deposition of YSZ thin film applied to thin-film fuel cell with high deposition rate and good quality. Reactive sputter deposition is a unique technique for depositing YSZ thin films at low temperatures (< ~573 K) because other techniques involving chemical reaction such as spray pyrolysis, CVD, etc., generally require much higher working temperature (>873 K). Also, by applying the bias voltage to the substrate during the sputter deposition, the deposited YSZ thin film could show the characteristics of high density film with less leakage current and pinholes and the increase of adhesion property.[19]

In this study, deposition characteristics and physical properties of YSZ thin films deposited by rf magnetron reactive sputtering were investigated. Also, thin-film-type YSZ oxygen sensor cells using Ni-NiO as the reference electrode have been fabricated for the first time with an optimized YSZ deposition condition and the gas sensing characteristics of YSZ thin films were studied.

Experimental

YSZ thin films were deposited at room temperature on Pt/NiO-Ni/SiO_2 substrates to characterize films properties using a rf/dc magnetron sputter deposition system with 7.62 cm diameter targets shown in Fig. 1. Zirconia stabilized with 8 mol % yttria (Y_2O_3) (99.9% purity), Ni (99.99% purity), and NiO (99.99% purity) were used as sputter targets for the deposition of YSZ and Ni-NiO mixed layer, respectively. The wafer holder of this equipment could be rotated for uniform and mixed layer deposition and also could be rf biased. In this experiment, 300 W of rf power was used to deposit YSZ thin films and rf-bias voltage of −45 V was applied at the holder to improve the density and adhesion of YSZ thin film. The base pressure was kept below 6.67×10^{-3} Pa before introducing sputtering gases for the deposition. Ar was used as the main sputtering gas, and a small amount of oxygen (5~20%) was added to reduce oxygen deficiency in the deposited YSZ thin films. The total flow rate of Ar(or Ar/O_2)

* Electrochemical Society Active Member.
z E-mail: jobae@nature.skku.ac.kr

S0013-4651(99)08-061-1 CCC: $7.00

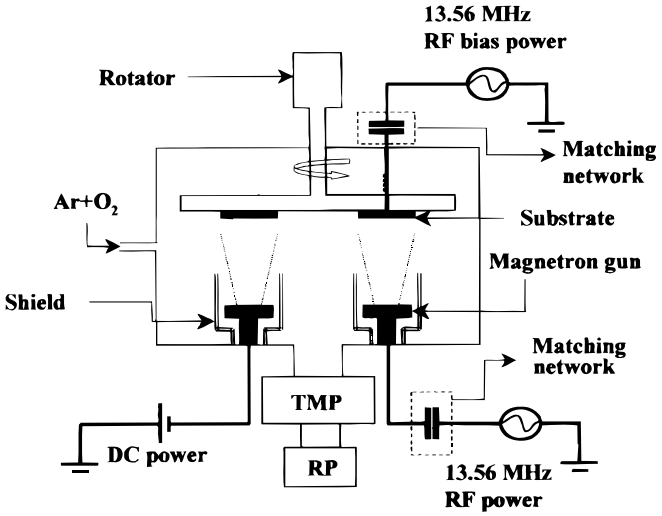

Figure 1. Schematic diagram of a four-target rf/dc magnetron sputter system.

and operating pressure was fixed at 20 cm^3/min and 1.333 Pa, respectively. The thickness of the deposited YSZ films was kept near 1 μm for the application of combustion control oxygen gas sensor.

To investigate gas-sensing characteristics of YSZ, the Ni-NiO reference layer was deposited on SiO_2 substrates followed by the deposition of multilayer (Pt/YSZ/Pt) composed of YSZ and Pt electrodes. The Ni-NiO reference layer was deposited by the co-sputtering of Ni by dc magnetron sputtering of 80 W and NiO by rf magnetron sputtering of 400 W using 6.67×10^{-1} Pa of Ar. During the co-sputtering, the substrate was rotated at 30 rpm. After the deposition, the Ni-NiO reference layer was annealed from 573 to 973 K in an oxygen environment using a tube furnace before the deposition of the multilayer to stabilize the Ni-NiO electrode. The Pt electrodes located at the top and bottom of the YSZ layer were deposited with the thickness of 200 nm by dc magnetron sputtering using at 6.67×10^{-1} Pa of Ar and 110 W of dc power. Specially designed shadow masks were used to form the required shape of the sensor cells. The gas-sensing test was carried out using the SiO_2/Ni-NiO/Pt/YSZ/Pt film structure in a sealed furnace by continuously flowing N_2, containing various percents of O_2, and by varying the operating temperatures. from 573 to 973 K. The oxygen partial pressure was in the range from 1.013×10^3 to 1.013×10^5 Pa. The oxygen pressure was calibrated by adjusting oxygen and nitrogen mass flowmeter while keeping the total flow rate at 100 cm^3/min. The measurement of electrochemical characteristics of the cells was performed by an electrometer (HP-34401A) and a potentiostat (EG&G PAR).

Results and Discussion

YSZ thin film.—Figure 2 shows the rf sputter deposition rates of YSZ as a function of Ar/O_2 gas mixture at 300 W of rf power and at 20 cm^3/min of total gas flow rates with and without applying −45 V of rf bias to the substrate. As shown in the figure, the increase of oxygen percent in the sputtering gas decreased the YSZ deposition rates from 350 nm/h with Ar only to about 130 nm/h with 30% of the oxygen in the sputtering gas. However, as shown in the figure, the application of self-bias voltage to the substrate increased the YSZ deposition rate. The decrease of deposition rate with the increase of oxygen percent in the sputtering gas appears to be related to the lower sputter yield of oxygen compared to that of Ar.[20] The increase of deposition rate with the increase of bias voltage to the substrate holder is possibly related to the increase of the target sputtering rate by the additional increase of the ionization rate of the sputtering gas through the increased secondary-electron injection to the target from the substrate as suggested by Green *et al*.[21] The application of rf bias to the substrate improved the adhesion of YSZ to the substrate when measured by the scratch test, and improved the density of the material. Also, by applying the rf bias voltage, the deposited YSZ thin

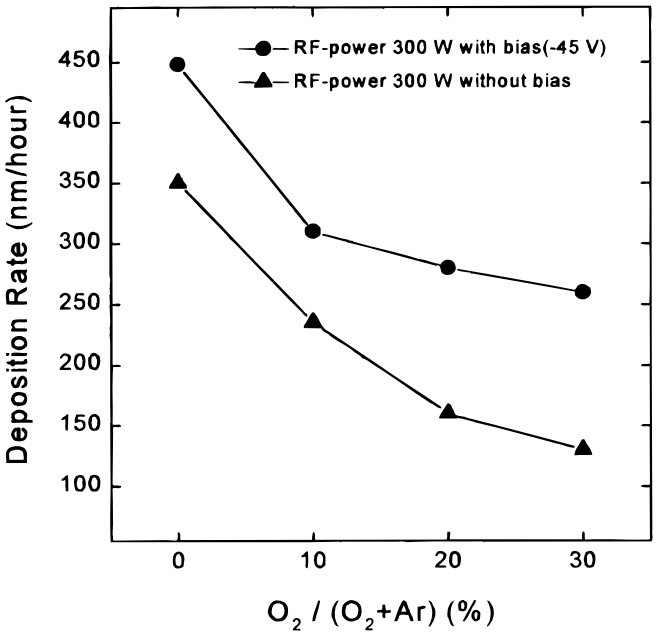

Figure 2. Deposition rates of YSZ thin film as a function of $O_2/(O_2 + Ar)$ with and without −45 V of substrate bias.

film showed fewer pinholes and therefore, less leakage current between the electrodes in the structure of Pt/YSZ/Pt. The addition of a small amount of oxygen in the plasma also improved the decrease in the leakage current of Pt/YSZ/Pt structure. Figure 3 shows the surface morphology of the deposited YSZ thin films as a function of oxygen percent while applying 300 W of rf power, 20 cm^3/min of total gas flow rate, and −45 V of rf bias. The addition of oxygen to Ar decreased the surface roughness of the deposited YSZ compared to the case with Ar only by decreasing the size of crystals on the surface as shown in Fig. 3, even though no significant differences in the surface roughness could be observed in the 10, 20, and 30% oxygen

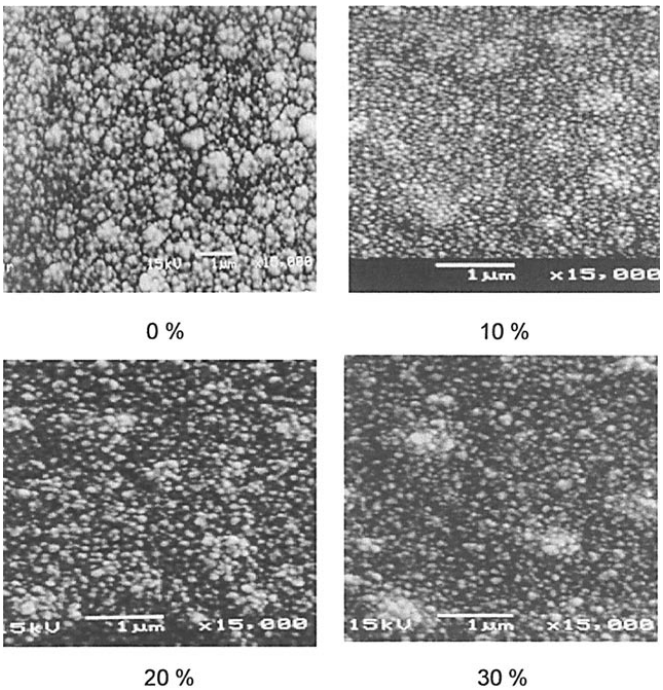

Figure 3. SEM images for YSZ thin film as a function of $O_2/(O_2 + Ar)$ with –45 V of substrate bias.

S0013-4651(99)08-061-1 CCC: $7.00

additions. The composition and structure of the deposited YSZ thin films were investigated using energy dispersive X-ray (EDX) and X-ray diffractometry (XRD), respectively. Figure 4 shows EDX data on the composition of YSZ thin films deposited as a function of the percent of oxygen in the sputtering gas. As shown in the figure, the composition of the YSZ thin film was almost independent of the percent of oxygen in the sputtering gas, therefore, was similar when measured using EDX. Figure 5a and b show the structure of YSZ thin films measured as a function of oxygen percent and the thickness of the YSZ thin film. The structure of fabricated YSZ thin films was the simple cubic structure that is typically observed for fully stabilized YSZ as suggested by Pawlewicz *et. al.*[22] for the zirconia-containing 7 to 47 mol % of yttria. (111), (200), and (220) cubic peaks were observed, and their peak ratios were similar to the peak ratios observed for YSZ powder, therefore, no preferred orientation was observed for our YSZ thin films.

Ni-NiO reference layer.—To fabricate a combustion control YSZ oxygen sensor, a multilayer thin film composed of SiO_2 substrate/Ni-NiO/Pt/YSZ/Pt has been used in this study. Among these multilayer thin films, the Ni-NiO layer is a material deposited as a reference for the standard oxygen concentration in the measurement of electromotive force of the oxygen sensor cell. To fabricate a stable YSZ sensor, the Ni-NiO layer needs to be chemically stable, therefore, the oxygen concentration of the Ni-NiO mixed layer should not be changed during the measurement of electromotive force using the oxygen sensor cell.

In this study, the Ni-NiO layer was deposited using a co-sputtering technique and the ratio of O/Ni was 0.43 as the deposited state, therefore, a metal-rich thin film was formed. This deposited film should be chemically stable at the operation temperatures (573 to 973 K) and environments (mixtures of O_2 and N_2). Therefore, after the deposition of the Ni-NiO layer, the Ni-NiO film was annealed for 30 min in a furnace at the temperature range from 573 to 973 K and in the oxygen environment (10 cm^3/min oxygen flow), and the ratio of O/Ni was measured using EDX. The result is shown in Fig. 6a. As shown in the figure, the ratio of O/Ni was increased as the annealing temperature was increased, however, at the temperature above 873 K the ratio of O/Ni appeared to be saturated. The ratio of O/Ni after the annealing at 873 K was 1.95, therefore, oxygen-rich film was obtained after the annealing.

To investigate the stability of Ni-NiO layer, the Ni-NiO layer was annealed up to 10 h at 873 K in the oxygen environment described above, and the change of O/Ni ratio was measured. The result is shown in Fig. 6b and, as shown in the figure, the ratios of O/Ni after the annealing from 30 min to 10 h remained similar, therefore the annealing at 873 K for 30 min appeared to be enough for the stabilization of the Ni-NiO layer to be used as the oxygen standard layer for the oxygen sensor cell investigated in our study.

SiO_2 substrate/Ni-NiO/Pt/YSZ/Pt cell.—Using the Ni-NiO layer annealed at 873 K for 30 min, the oxygen sensor cell composed of SiO_2 substrate/Ni-NiO/Pt/YSZ/Pt was fabricated and the electromotive force of the cell was measured as a function of the oxygen percent in O_2/N_2 environments at different operating temperatures from 573 to 973 K. In the case of YSZ, YSZ deposited with Ar/10% O_2 was used to fabricate the above cell as the initial estimation of YSZ

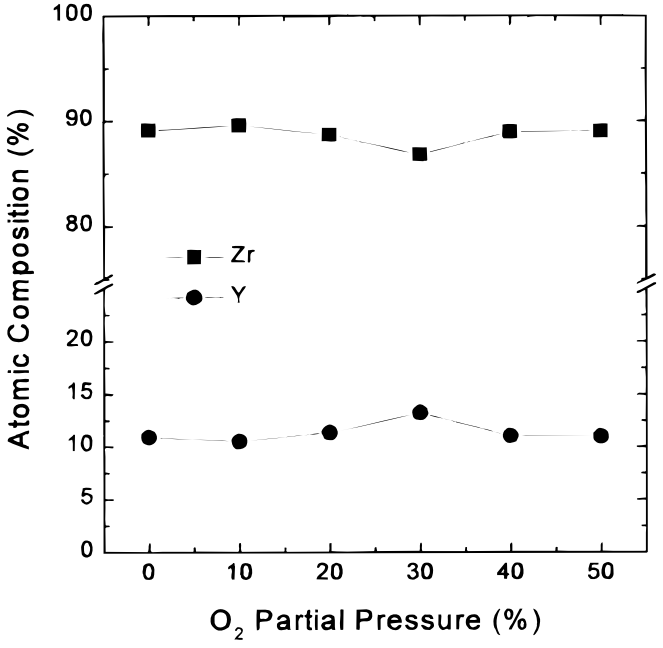

Figure 4. EDX data on the composition of YSZ thin films deposited as a function of oxygen partial pressure in the sputtering gas.

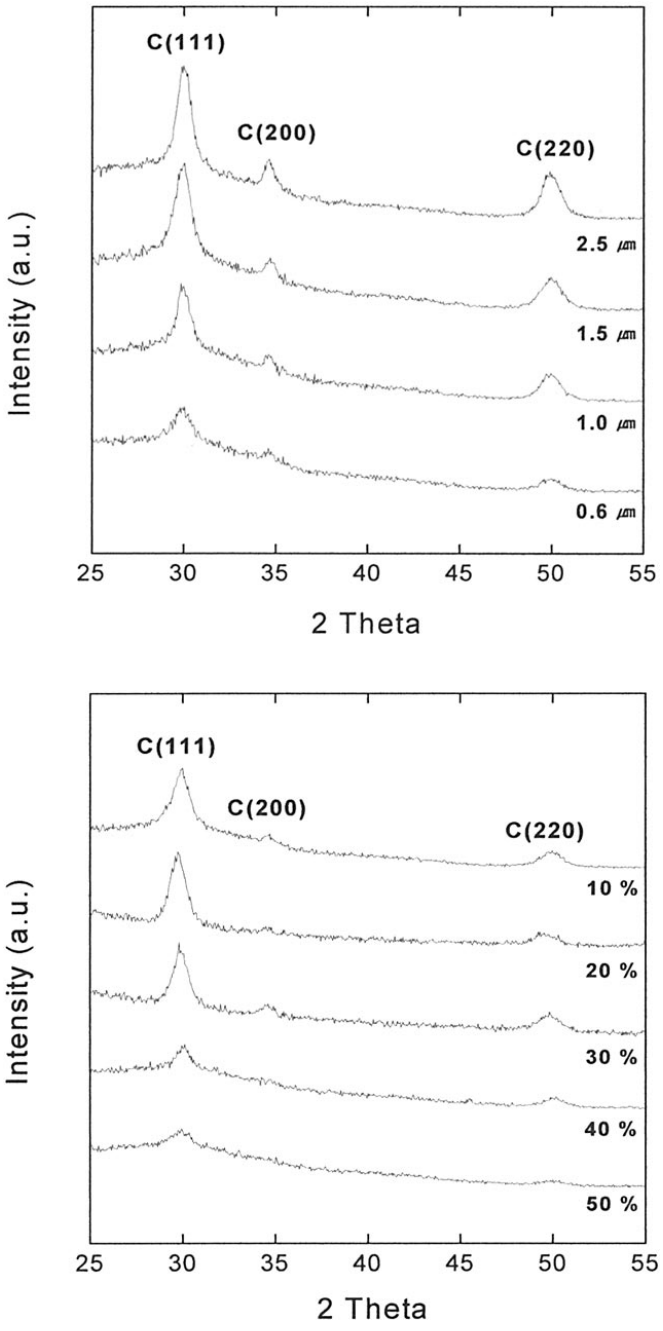

Figure 5. XRD data of YSZ thin films for various thicknesses (a, top) and oxygen partial pressure in the sputtering gas (b, bottom).

S0013-4651(99)08-061-1 CCC: $7.00

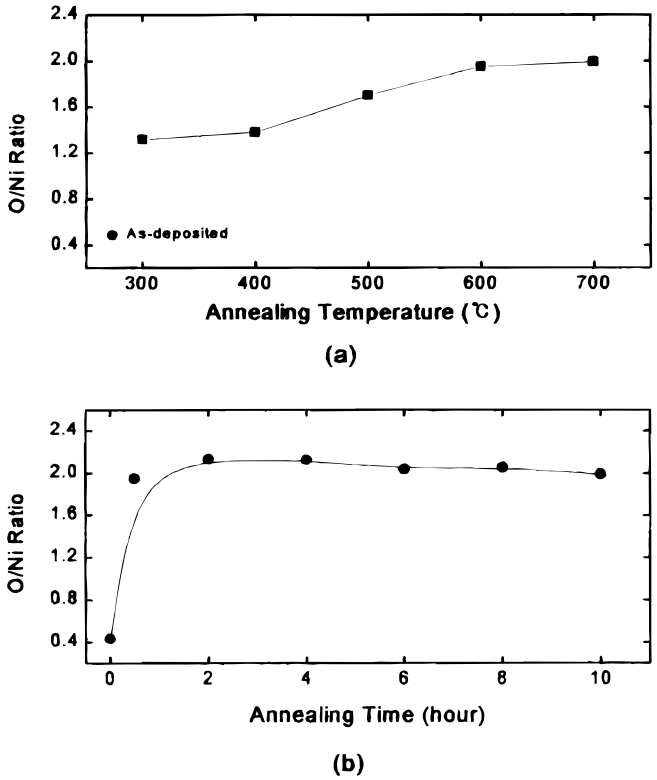

Figure 6. Variation in the O/Ni ratio of Ni-NiO layer as a function of annealing temperature (a) and time (b).

thin-film oxygen sensor. When the EMF of the oxygen sensor was measured at 573 K, less than 2 mV of EMF was observed for different oxygen partial pressures (theoretically calculated value by the Nernst's equation is 56.6 mV at p_{O_2}:1,013 Pa). This low EMF is possibly due to that low ion diffusion rate of the oxygen in the cell at the low temperature. Because the diffusion of the oxygen ion through YSZ thin film is obtained by the diffusion of the oxygen vacancy in the film, higher temperatures which can enhance the mobility of the oxygen vacancy may be required for improving the diffusivity of oxygen ions. Also, from the Nernst's equation described below, the operation temperature is proportional to the EMF. Therefore, it is one of the important parameters controlling the conductivity and diffusivity of oxygen ions. Figure 7 shows the EMF of the cell measured at 773 K as a function of time for different oxygen partial pressures in the O_2/N_2 environment. As shown in the figure, a certain stabilizing time related to the oxygen diffusion through the cell appears to be required at a given oxygen partial pressure to obtain a steady-state EMF. However, a high and reproducible EMF was obtained at different oxygen partial pressures. Figure 8 shows the measured EMF as a function of oxygen partial pressure at 673 and 773 K. As references, theoretical EMF values were calculated and were included in the figure. The following Nernst's equation was used for the calculation of the theoretical EMF [23]

$$EMF = \frac{RT}{4F} \ln \frac{p_{O_2(I)}}{p_{O_2(II)}}$$

where R is gas constant (8.3144 J/mol), T is operating temperature in kelvin, and F is Faraday constant. $p_{O2(I)}$ is the reference oxygen concentration of Ni-NiO and, at $T = 773$ K, $p_{O2(I)}$ is $\sim 1 \times 10^5$ Pa, and $p_{O2(II)}$ is oxygen percent in the O_2/N_2 environment. As shown in the figure, the measured EMF values decreased logarithmically as the oxygen partial pressure was increased and were reasonably close to the theoretical EMF values calculated, especially for the temperatures between 673 and 773 K.

Figure 9 shows the EMF values measured at 873 K as a function of time for different oxygen partial pressures. In this case, even though some EMF values are observed, the EMF values were significantly low compared to the theoretically calculated EMF values and were not stable. The low and unstable EMF appears to be from the structural change of the materials and the instability between the layers in the multilayers of the SiO_2 substrate/Ni-NiO/Pt/YSZ/Pt at the high operating temperature. Especially, the Ni-NiO mixed layer showed the structural change from amorphous to crystalline at 873 K even though there was no compositional change observed as shown in Fig. 6b. Figure 10 shows the X-ray diffraction data measured for the Ni-NiO layer after annealing at various temperatures for 30 min.

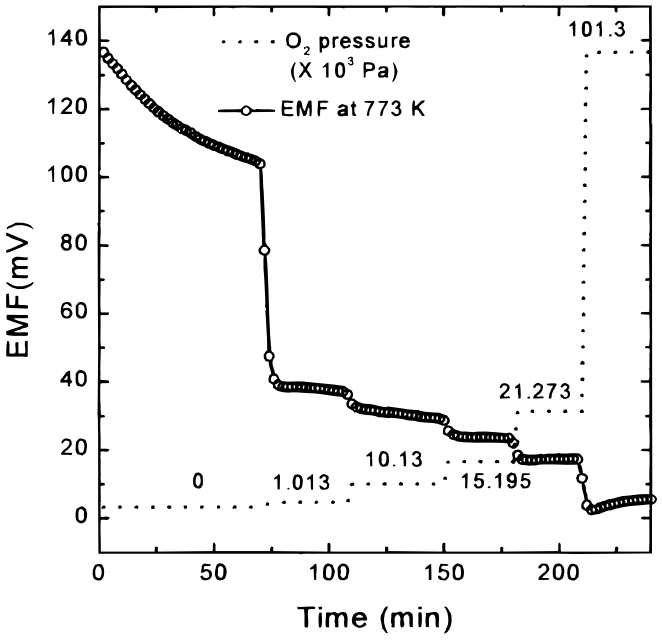

Figure 7. Sensing characteristics of the fabricated YSZ oxygen gas sensor cell as a function of oxygen partial pressure at 773 K.

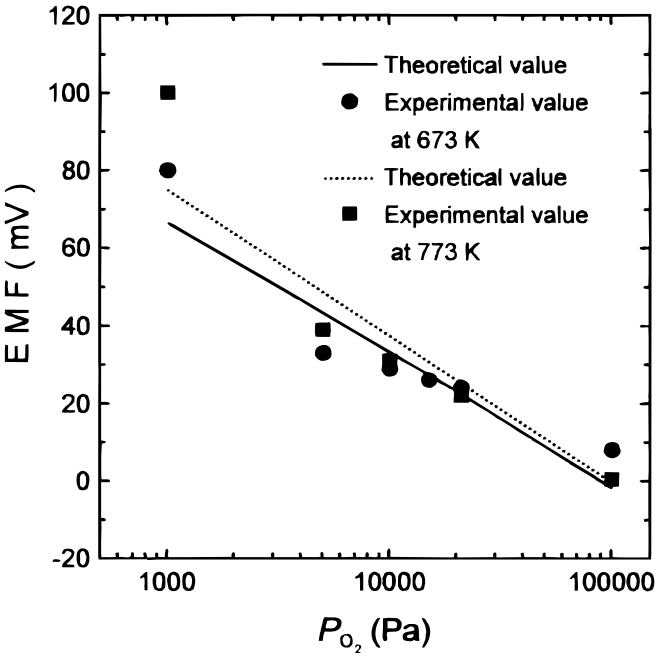

Figure 8. Calculated theoretical EMF values and experimentally measured EMF values as a function of oxygen partial pressure at 673 and 773 K, respectively.

S0013-4651(99)08-061-1 CCC: $7.00

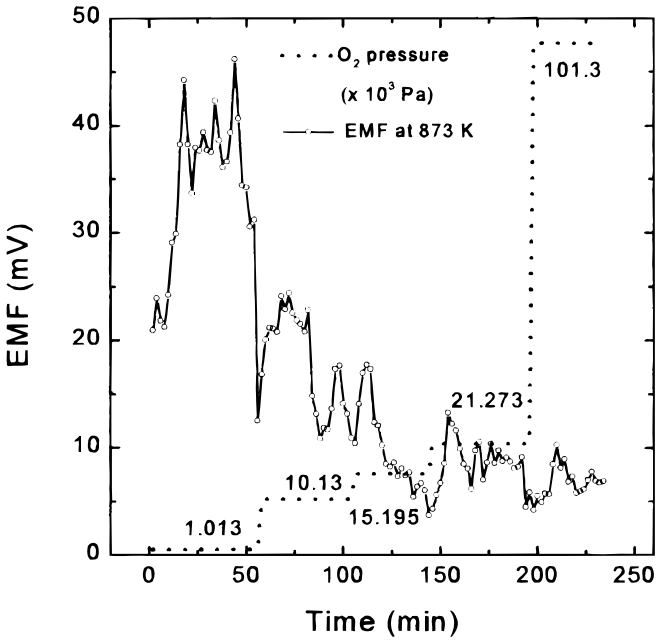

Figure 9. Sensing characteristics of fabricated YSZ oxygen gas sensor cell at 873 K as a function of oxygen partial pressure.

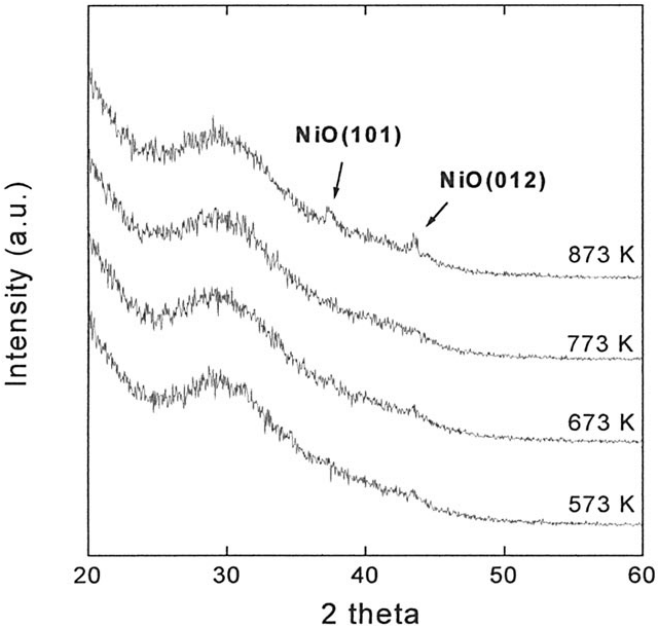

Figure 10. XRD data of Ni-NiO as a function of annealing temperature.

As shown in the figure, until the annealing to 773 K, the Ni-NiO layer remained as amorphous. However, when the annealing temperature increased to 873 K, some of the Ni-NiO layer was crystallized. The crystallization of the materials consisting of the multilayers will increase the roughness of the interface and will change the interface properties. Therefore, the measured EMF will be unstable as we observed in Fig. 9 for the cell operating at 873 K. When the cell was operated at 973 K, the cell appeared to be shorted and no EMF was observed, possibly due to the enhanced unstability of the interface and interdiffusion between the layers (not shown).

Conclusions

Thin film oxygen gas sensor based on 8 mol % yttria-stabilized zirconia was fabricated using a four-target rf/dc magnetron sputtering system. The cell structure used had a SiO_2 substrate/Ni-NiO/Pt/YSZ/Pt. YSZ thin film was deposited using rf sputtering in 10% oxygen mixed with Ar and by rf biasing at −45 V. The rf biasing and mixture with oxygen improved the adhesion and density of deposited YSZ. The Ni-NiO layer used for the oxygen standard reference was deposited by co-sputtering and annealed at 873 K for 30 min in an oxygen environment for improving the stability of the reference layer at the operating temperature.

EMF values were measured using the fabricated oxygen cell at the temperature in the range from 573 to 973 K while varying the oxygen partial pressure in an O_2/N_2 atmosphere. The measured EMF values were logarithmically decreased with increasing oxygen partial pressure and were increased with the increase of operational temperature in general. The measured EMF values were compared with the theoretically calculated EMF values described by Nernst's equation. The measured EMF were close to the calculated EMF for the temperature range from 673 to 773 K. When the operating temperature was 573 K, an EMF lower than the theoretically calculated value was obtained, possibly due to the low diffusion rate of oxygen. When the operating temperature was higher than 873 K, the EMF again was lower than the calculated values and was unstable, possibly due to structural changes of the materials and instability of the interfaces of the multilayer cell structure. The best oxygen sensing properties of the fabricated cell were obtained at the operation temperature of 773 K.

Sungkyunkwan University assisted in meeting the publication costs of this article.

References

1. T. Usui, H. Yamamoto, K. Ishibashi, and M. Nakazawa, *J. Appl. Phys.*, **29**, 606 (1990).
2. S. P. S. Badwal, *Appl. Phys.*, **A50**, 449 (1990).
3. A. M. Azad, S. A. Akbar, S. G. Mhaisalkar, L. D. Birkefeld, and K. S. Goto, *J. Electrochem. Soc.*, **139**, 3690 (1992).
4. C. Nylander, *J. Phys. E; Sci*, *Instrum.*, **18**, 736 (1985).
5. K. Saji, H. Kondo, and J. Takahashi, *Sens. Actuators B*, **13-14**, 695 (1993).
6. N. Miura, T. Raisen, G. Lu, and N. Yamazoe, *J. Electrochem. Soc.*, **144**, L198 (1997).
7. W. D. Kingery, J. Pappis, M. E. Doty, and D. C. Hill, *J. Am. Ceram. Soc.*, **42**, 393 (1959).
8. J. Weissbart and R. Ruko, *J. Electrochem. Soc.*, **109**, 723 (1962).
9. T. Usui, H. Yamamoto, K. Ishibashi, and M. Nakazawa, *Jpn. J. Appl. Phys.*, **29**, 606 (1990).
10. T. Kenjo and T. Nakagawa, *J. Electrochem. Soc.*, **143**, L92 (1996).
11. T. J. Mazanec, *Electrochem. Soc., Interface*, **5**, 46 (1996).
12. N. Miura, T. Raisen, G. Lu, and N. Yamazoe, *J. Electrochem. Soc.*, **144**, L198 (1997).
13. G. Velasco, J. Ph. Schnell, and M. Croset, *Sens. Actuators*, **2**, 371 (1982).
14. N. R. Shankar, H. Herman, and S. P. Singhal, *Thin Solid Films*, **119**, 159 (1984).
15. Y. Takahashi, T. Kawae, and M. Nasu, *J. Cryst. Growth*, **74**, 409 (1986).
16. D. Y. Kim, C. H. Lee, and S. J. Park, *J. Mater. Res.*, **11**, 2583 (1996).
17. E. T. Kim and S. G. Yoon, *Thin Solid Films*, **227**, 7 (1993).
18. M. Balog, M. Schieber, M. Michman, and S. Patai, *J. Electrochem. Soc.*, **126**, 1203 (1979).
19. T. Tsai and S. A. Barnett, *J. Electrochem. Soc.*, **142**, 3084 (1995).
20. M. Ohring, *The Materials Science of Thin Films*, p. 128, Academic Press, Hoboken, NJ (1992).
21. J. E. Greene, R. E. Klinger, L, B, Welsh, and F. R. Szofran, *J. Vac. Sci. Technol.*, **14**, 177 (1977).
22. W. T. Pawlewicz and D. D. Hays, *Thin Solid Films*, **94**, 31 (1982).
23. A. M. Azad, S. A. Akbar, S. G. Mhaisalkar, L. D. Birkefeld, and K. S. Goto, *J. Electrochem. Soc.*, **139**, 3690 (1992).